Carbon 137 (2018) 118–124

Contents lists available at ScienceDirect

Carbon

journal homepage: www.elsevier.com/locate/carbon

Substrate effect on electrical conductance at a nanoasperity-graphene contact

Xiaoli Hu [a], Jihyung Lee [b], Diana Berman [b, c, *], Ashlie Martini [a, **]

[a] Mechanical Engineering, University of California Merced, Merced, CA, 95343, United States
[b] Materials Science and Engineering, University of North Texas, Denton, TX, 76203, United States
[c] Advanced Materials and Manufacturing Processes Institute, University of North Texas, Denton, TX, 76203, United States

ARTICLE INFO

Article history:
Received 27 February 2018
Received in revised form
20 April 2018
Accepted 12 May 2018
Available online 14 May 2018

ABSTRACT

The use of graphene for applications such as micro- and nano-scale electronic devices often involves incorporating the two-dimensional material onto various substrates. However, the effects of the substrate's mechanical properties on electrical contact conductance are not fully understood. Here, we explore these effects by measuring the conductance between a nanoscale probe and a single layer of graphene with three different levels of substrate support: no substrate, i.e. free-standing graphene, an elastic substrate, and a rigid substrate. These three systems are studied using conductive atomic force microscopy experiments complemented by molecular dynamics simulations using the electrochemical dynamics with implicit degrees of freedom method. In both experiments and simulations, at a given normal force, current increases as: rigid substrate < elastic substrate < no substrate. We demonstrate that the substrate support influences graphene/tip contact conductance through substrate's elasticity, which determines contact size, as well as through variability of interatomic distances in the contact, which contributes to the interface resistivity.

1. Introduction

Graphene is a two-dimensional material that has gained significant attention due to its unique electrical, mechanical, thermal and tribological properties [1–4]. These properties enabled incorporation of graphene into many different applications, such as biosensors, electronic devices, electromechanical resonators and composites [5–10]. Often, the atomically thin nature of graphene requires depositing it on a substrate, which may in turn significantly affect the graphene's physical properties [11]. For example, an insulating substrate affects the in-plane carrier mobility of graphene, which may result in an increase of the electrical conductivity of the graphene [12]. The interactions between a substrate and graphene affects graphene's chemical reactivity [13,14], electronic properties [15,16], and shear strength and work of adhesion [17]. In addition to changing graphene's intrinsic properties, a substrate can affect the properties of the contact between graphene and an adjacent material, such as electrical contact conductance [18].

The effect of a substrate on electrical contact conductance is of particular interest for applications such as microelectromechanical systems (MEMS) and nanoelectromechanical systems (NEMS), where nanoscale contacts between graphene and an adjacent material enable conduction within the device. Though MEMS involve multi-asperity contacts, their electrical transport may be extrapolated from single asperity contact experiments, traditionally performed using atomic force microscopy (AFM). Conductive AFM enables measurement of current flow through the contact formed by a nanoscale probe and the surface of interest in a controlled manner [19]. Previous studies using this approach have shown that electronic transport at an AFM tip-sample contact is determined largely by the magnitude of the applied normal force and the elastic and plastic responses of the material to that force [20,21]. Additionally, it was reported that defects in the contact can affect conduction [22]. For graphite specifically, studies have shown that contact resistivity can be dependent on the thickness of the graphite and topographic features induced by the substrate [23,24].

* Corresponding author. Materials Science and Engineering, University of North Texas, Denton, TX, 76203, United States.
** Corresponding author. Mechanical Engineering, University of California Merced, Merced, CA, 95343, United States.
E-mail addresses: diana.berman@unt.edu (D. Berman), amartini@ucmerced.edu (A. Martini).

https://doi.org/10.1016/j.carbon.2018.05.028
0008-6223/

However, there is a lack of understanding of how the mechanical properties of the substrate affect the conductance of a nanoscale contact between graphene and another electrically conductive material. In this study, we provide a detailed analysis of a substrate's contribution to the stable electrical contact between graphene and a conductive AFM tip.

We isolate the effect of the substrate by measuring conductance between a nanoscale conductive probe and graphene, where the single layer of graphene has three different levels of substrate support. The concept is illustrated in Fig. 1. The cases studied are: (a) no substrate, i.e. free-standing graphene, (b) an elastic substrate, and (c) a rigid substrate. These three systems are studied using conductive AFM experiments complemented by molecular dynamics (MD) simulations. In the experiments, current is measured using a doped ultrananocrystalline diamond (UNCD) tip in contact with free-standing graphene, graphene on polydimethylsiloxane (PDMS) and graphene on UNCD. In the complementary simulations, current is calculated using MD with the electrochemical dynamics with implicit degrees of freedom (EChemDID) method [25,26] for free-standing graphene, graphene on graphite and graphene on diamond. In both experiments and simulations, current is obtained as a function of normal force and the differences between the three cases are evaluated. The simulations allow further analysis of the origin of observed differences, in terms of the continuum concept of elasticity as well as local atomic-scale effects.

2. Methods

Electrical current flow as a function of normal force and voltage bias was measured for free-standing graphene, graphene supported by PDMS, and graphene supported by UNCD. The substrates were chosen from nonconductive materials to eliminate any possible cross conductivity contribution from the substrate. The hardness of substrate materials was measured with a Vickers hardness machine and found to be 49 GPa for the UNCD and 0.97 GPa for the PDMS. These results are comparable to values reported previously for these materials: UNCD (65–95 GPa [27]) and PDMS (1.57 GPa [28]). Therefore, the hard substrate was approximately 50 times harder than the soft substrate in these experiments. Statistically it has been shown that, the harder the substrate, the larger the elastic modulus [29,30]. Thus, the graphene supported by UNCD is expected to be the most rigid of the three cases.

To prepare the samples, single layer graphene was first chemical vapor deposition (CVD) grown on a copper foil and then transferred on the substrate of interest using 200 nm thick polymethyl(methacrylate) (PMMA) film. During the transfer, the copper was etched in a copper etchant (Sigma Aldrich) and the resulting graphene with the PMMA film on top was transferred to the substrate. The PMMA was removed using a warm acetone bath. Complete removal of the PMMA layer and the single-layer nature of the graphene film were confirmed using scanning electron microscopy (SEM) and Raman spectroscopy with a 534 nm green laser. For the free-standing case, the graphene was transferred onto a silicon nitride substrate with 2 μm diameter holes as shown in Fig. 2(a). For elastic substrate measurements, the monolayer graphene film was transferred onto a PDMS substrate as shown in Fig. 2(b). For rigid substrate measurements, the monolayer graphene film was transferred onto a UNCD substrate, as shown in Fig. 2(c), grown using Hot Filament UNCD synthesis technique [31].

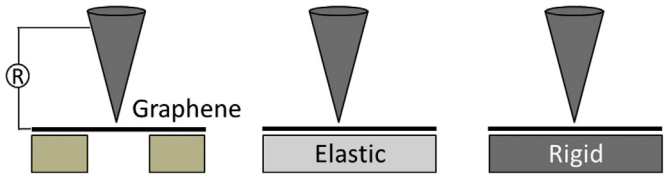

Fig. 1. Schematic of the conceptual design. Current is measured for a nanoscale tip brought into contact with (a) free-standing graphene, (b) graphene supported by an elastic substrate and (c) graphene supported by a rigid substrate. (A colour version of this figure can be viewed online.)

The samples were attached to the insulating quartz substrate using a ceramic paste and the grounding connection was made on the edge of the samples using a conductive silver paint. This geometry was created to allow the electrical current to travel from the tip to the graphene and then laterally across the graphene film to the contacting pads. The electrical resistance of the conductive pads was measured to be on the order of 1 Ohm, which is substantially lower than the contact resistance obtained from I-V curves measured in the experiments.

AFM measurements were performed using a Bruker Multimode AFM in contact mode with a conductive doped UNCD tip (Advanced Diamond Technologies, spring constant of ~0.3 N/m, tip radius is ~20 nm), shown in Fig. 2(d). High mechanical strength and wear resistance of the diamond tip allowed multiple tests to be performed without detectable changes of the tip radius. Interchangeability of the tip was also confirmed by performing several cycles of measurements in the following order: free-standing, PDMS, UNCD, PDMS and free-standing. The evolution of the electrical contact between the tip and graphene was tested in static mode while increasing the applied normal force. The maximum normal force was limited to 250 nN, which remained well below critical normal forces required for free-standing CVD grown graphene rapture (order of 2000 nN) or for inelastic deformation under AFM nanoindentation [32,33]. The applied bias voltage varied from −2 V to 2 V and the maximum electrical current flow was limited to a maximum of 1 μA to prevent local heating-induced failure of the tip and melting of the PDMS substrate.

To complement the experimental studies, we developed atomistic models of a diamond tip (radius 3 nm, height 2 nm) approaching three substrates: suspended monolayer graphene, eight-layer graphite, and monolayer graphene supported by a diamond substrate as shown in Fig. 3(a)-(c). These are comparable to the experimental systems shown in Fig. 2 except that, for the elastic substrate, instead of PDMS, the simulations used graphite for simplicity and model availability. Although the elastic modulus of graphite is not the same as PDMS, the elastic modulus of both materials is smaller than that of UNCD. Therefore, both graphite and PDMS represent an intermediate case between the unsupported free-standing graphene and the rigid diamond substrate.

The lateral dimensions of all model systems were 9.7 nm × 8.4 nm. The atoms in the top 0.4 nm of the tip were treated as a rigid body. The atoms at the both ends of the graphene layer along one of the lateral directions were fixed in order to constrain movement. The boundary in the other lateral direction was periodic. For the graphite substrate system, the bottom layer of graphene was fixed. For the graphene/diamond substrate system, the thickness of the diamond was about 1 nm and the atoms in the bottommost 0.2 nm of diamond were held fixed. The interatomic interactions were described by the ReaxFF force field with parameters reported in Ref. [34]. A Langevin thermostat was applied to all the non-constrained atoms in the directions perpendicular to the direction of tip movement to control the temperature at 300 K. The simulations were performed with LAMMPS [35] and the timestep was 0.25 fs.

The entire system was first relaxed for 5 ps with the tip 1.2 nm away from the surface until the potential energy of the system was stable. Then the tip was moved down at a speed of 10 m/s towards the surface. At different vertical positions, the tip movement was

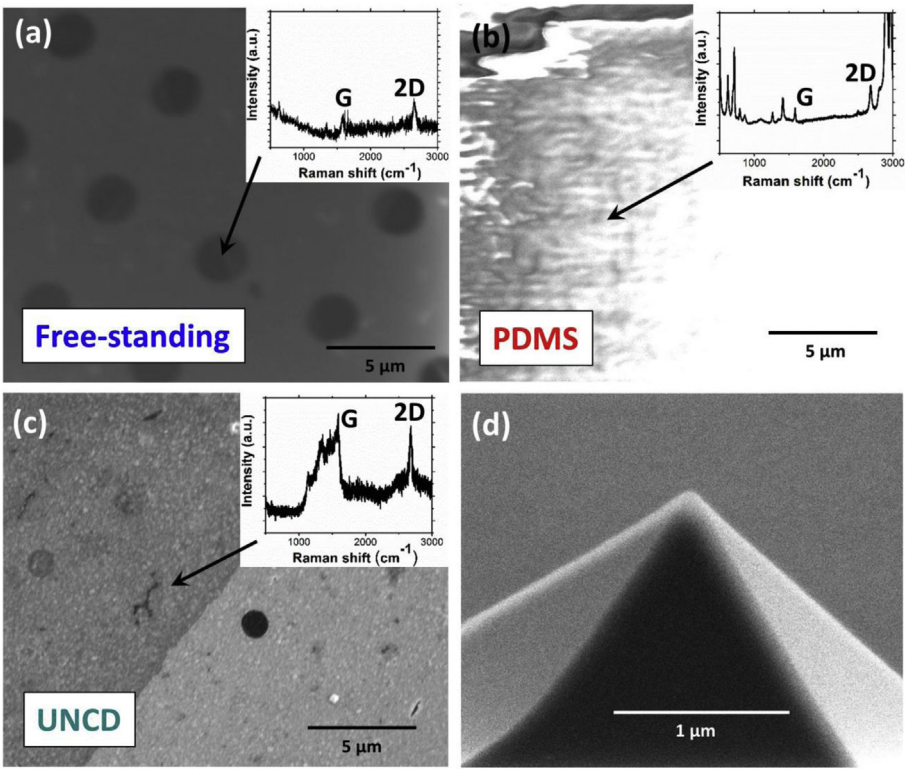

Fig. 2. SEM images of the (a) free-standing graphene, (b) graphene on the PDMS substrate, (c) graphene on the UNCD substrate, and (d) conductive UNCD tip. Raman spectra analysis in the insets confirms the successful transfer of the graphene single-layer film. (A colour version of this figure can be viewed online.)

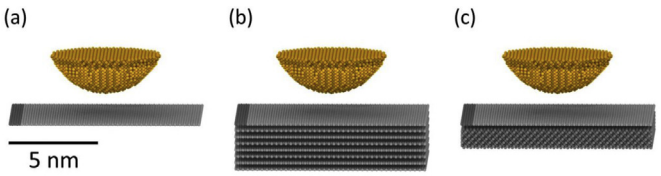

Fig. 3. In the simulation, the tip was brought into contact with (a) free-standing graphene, (b) graphite and (c) graphene supported by diamond. The darker color on the tip and graphene represents the positions of the electrodes, i.e. where the voltage difference was applied for the EChemDID method. (A colour version of this figure can be viewed online.)

stopped and the model was relaxed for 50 ps, during which the normal force was calculated by averaging the vertical force on the tip during the last 10 ps of steady state. We also estimated the contact area during relaxation. The atoms in the graphene layer that were within 0.4 nm from a tip atom were considered to be in contact. Then the contact area was obtained by multiplying the total number of contact atoms by the approximate area per atom, which was estimated to be 0.0262 nm^2. This approach to calculating contact area has been used previously [3,19,36]. The contact area was averaged over the last 10 ps during steady state.

EChemDID [25,26,37] was used to obtain conductance after system relaxation at each vertical tip position. This method calculates electrical current from the electrochemical potential of atoms in a reactive MD simulation and it has been successfully used to describe experimentally-observed electrical phenomenon and to predict the behavior of nanoswitches [25,26,36,37]. In EChemDID, the voltage applied to the electrodes propagates through the system following Maxwell's wave equations until the entire system is equilibrated and fictitious diffusive dynamics is used to describe the equilibration process. Joule heating and electron migration are not included in this calculation. Here, in order to isolate the conductance of the graphene, we removed the atoms in bottom seven-layers of the graphite and the diamond substrate, and froze the positions of the atoms in the graphene, before calculating current. A voltage difference of 2 V was applied to the atoms identified by a darker color in Fig. 3. Since the model does not capture Joule heating, the magnitude of the applied voltage does not affect trends in the calculated current, which is unitless and scales linearly with voltage. We confirmed that trends in the current results are independent of the applied bias in these simulations. The results are reported unitless because the conductivity of the interface is not known and so cannot be used to convert the EChemDID output to standard current units.

3. Results and discussion

In the experiment, the current for each of the three substrate cases was measured as a function of applied voltage and normal force. The results are shown in Fig. 4(a)-(c). It can be seen that the current increases with applied voltage for all three samples, but its dependence on the normal force varies with substrate type. To analyze the normal force dependence, the current at a voltage bias of 0.5 V was analyzed for the three cases, as shown in Fig. 4(d). At all except the smallest normal forces, the current is largest for the free-standing graphene and smallest for the UNCD-supported graphene.

From the simulations, the calculated current as a function of normal force is shown in Fig. 5. Note that the normal forces in the simulations are smaller than those in the experiments because of the smaller size of the model tip. Regardless, similar trends to those observed in the experiment (Fig. 4(d)) are found in the simulation. At the smallest normal forces, the current with the elastic substrate is greater than that for the free-standing graphene. However, at all other normal forces, the current increases as: rigid

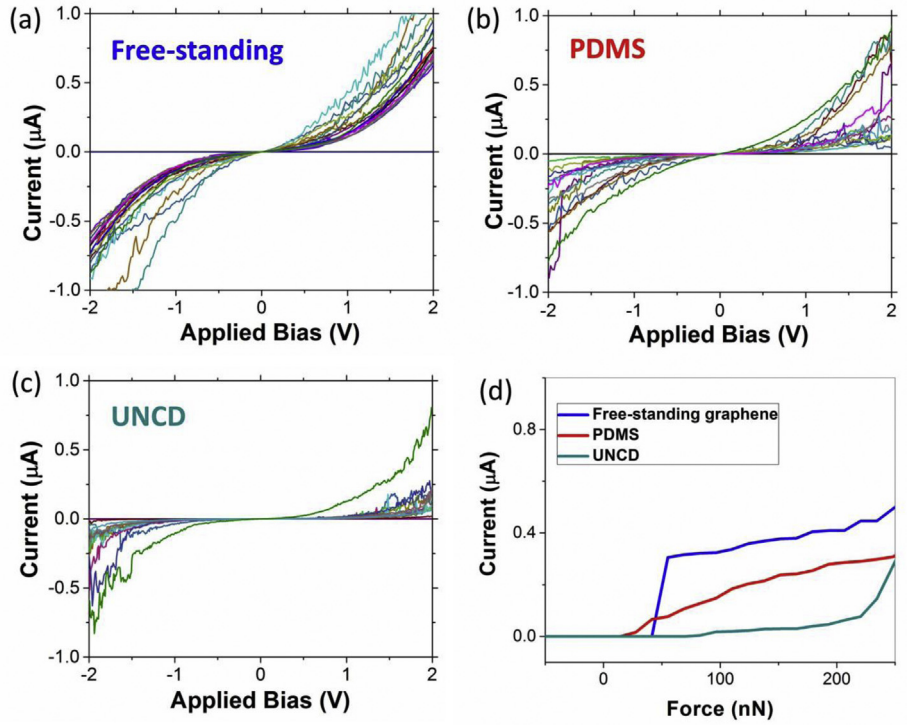

Fig. 4. Experimental measurements of current as a function of voltage bias (−2 to 2 V) at a range of normal forces (−50 to 250 nN) for: (a) free-standing graphene, (b) graphene on elastic PDMS substrate, and (c) graphene on rigid UNCD substrate. (d) Current as a function of normal force for the three cases at 0.5 V applied bias. (A colour version of this figure can be viewed online.)

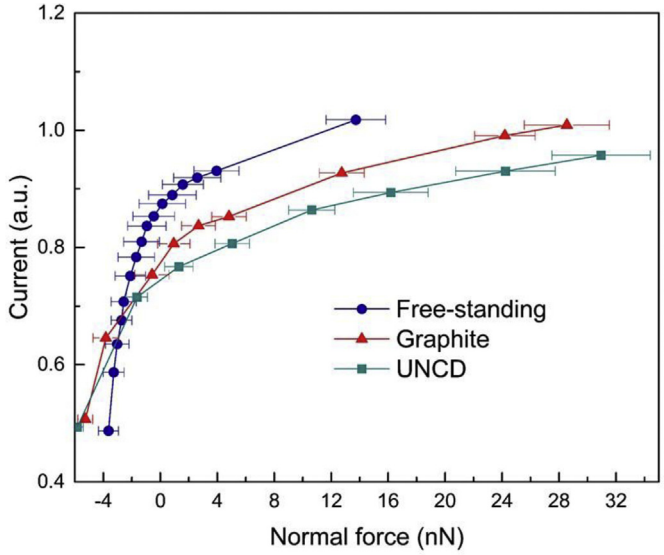

Fig. 5. Simulation results of an electrical current flow through the graphene/tip contact as a function of applied normal force for graphene on three different substrates, where the error bars represent standard deviation. (A colour version of this figure can be viewed online.)

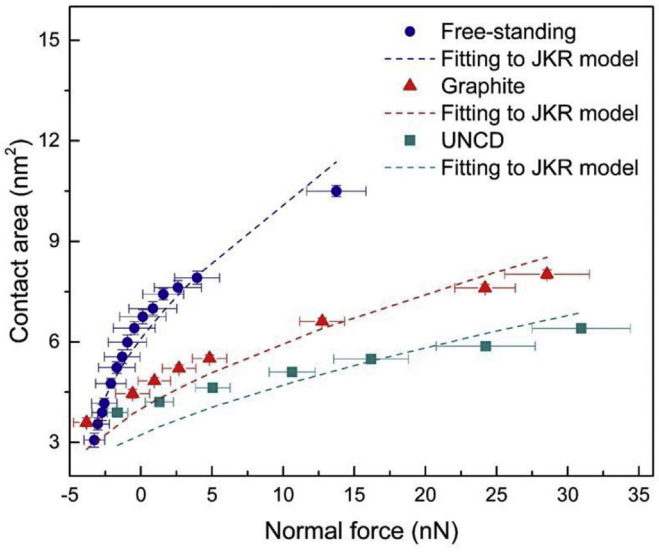

Fig. 6. Simulation results of the contact area as a function of the normal force, where the symbols represent simulation data and the dashed lines represent fits using the JKR model. (A colour version of this figure can be viewed online.)

substrate < elastic substrate < free-standing. This trend is the same as in the experiments and will be analyzed further next.

Since both the graphene and doped UNCD are conductive, the most significant factor determining current should be the size of the contact. Contact area as a function of normal force can be obtained directly from the simulations, as shown in Fig. 6. We observe that, as expected based on classical contact mechanics theories, contact area increases with increasing normal force [19]. Also, at the same normal force, the contact area is the largest for free-standing graphene and the smallest for graphene supported by the UNCD. One explanation for this, again in the context of continuum contact mechanics, might be the elasticity of the substrate. To evaluate this, we fit the relationship between contact area and normal force to obtain a value of the elastic modulus using the Johnson–Kendall–Roberts (JKR) model [38]. The JKR model has

been used previously to determine the elastic modulus of graphite in an AFM experiment [39] and it fits the simulation data here reasonably well (the JKR fits are shown as dashed lines in Fig. 6). Using this approach, we found that the out-of-plane elastic modulus for free-standing graphene, graphite, and graphene supported by UNCD are 11.6 GPa, 32.7 GPa, and 49.8 GPa, respectively. In the case of the graphite, reference data is available for comparison and our fit elastic modulus is within the range of values reported from previous experiments and simulations (30–44 GPa) [39–41], indicating this approach to estimate elastic modulus is reasonable. Therefore, the observation that the elastic modulus increases from the smallest value for the free-standing graphene to the largest value for the UNCD-supported graphene may explain the observed contact area trends.

The similar trends in the contact area (Fig. 6) and current (Fig. 5) data suggest that the contact area likely plays a major role in determining conductance for the three substrate cases. However, the difference in current between free-standing graphene and UNCD-supported graphene is not as large as the difference in contact area between those two samples. For example, at a normal force of ~5 nN, the current for the UNCD-supported graphene is 14% lower than that for the free-standing graphene, but the contact area is 41% smaller. This suggests that the substrate's influence on electrical current may be more than just its effect on contact size.

Classical electric contact resistance theories predict that current will decrease with resistivity and increase with contact area, where the contact area effect depends on the ratio of the size of the contact to the mean free path of electrons in the material [19]. Due to the high carrier charge mobility in graphene, the electron mean free path can exceed 10 μm [42], which is much larger than the contact radius in the simulation. This indicates that the electrical behavior should follow the Sharvin limit [43], in which conductance is linearly proportional to the contact area. This relationship provides a means of estimating resistivity from our simulation data. Specifically, we fit the Sharvin equation to the current and contact area data from simulation in a normal force range where the data is approximately linear, as shown in Fig. 7. We observe that the slope of the linear fit is largest for the UNCD-supported graphene, corresponding to the smallest resistivity. The current obtained from EChemDID does not have units, so actual resistivity values cannot be compared. However, the unitless resistivity of the UNCD-supported graphene is 17% smaller than that of the graphite, and 29% smaller than that of the free-standing graphene. To understand this trend, we take advantage of the atomic-scale details available in the simulation.

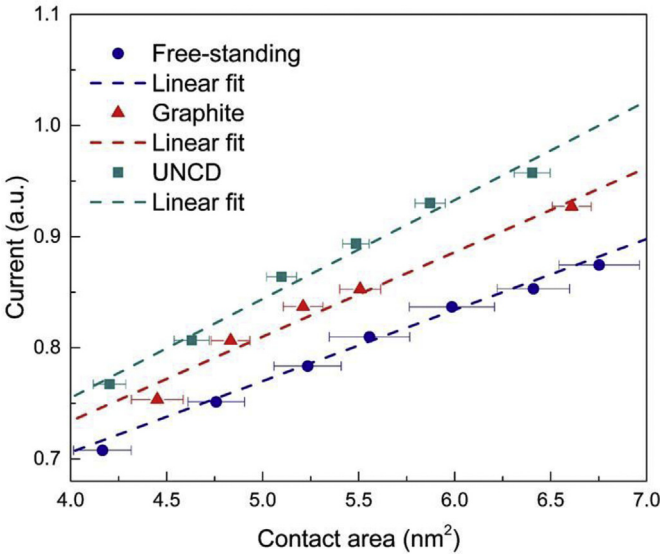

Fig. 7. Simulation results of the electrical current as a function of contact area, where the dashed lines show linear fits to the data. (A colour version of this figure can be viewed online.)

Previous studies have shown that graphene resistivity can change with material strain [44–48]. In graphene, it has been shown that resistivity increases with tensional strain in the elastic deformation region due to the increase in distance between atoms [45]. Therefore, we calculated the cumulative distribution function of in-plane atom-atom distances for atoms within the graphene contact area. The results are shown in Fig. 8(a) where we obseve that, at a smaller distance, the cumulative probabilities are larger for the UNCD-supported graphene than for the free-standing graphene. This corresponds to less tensional strain in the former and, in turn, lower resistivity. It has also been suggested the current going through an interface decays exponentially with the atom-atom distance across that interface [49,50]. This is quantified here by the cumulative distribution function of distances between atoms in the graphene contact area and atoms in the tip. The results are shown in Fig. 8(b). Like the in-plane distances, more of the atom distances across the interface are smaller for the UNCD-supported graphene. These shorter distances will correspond to more current and lower resistivty. Therefore, for the graphene on a more rigid substrate, the contact area is smaller due to the larger elastic modulus, which leads to a smaller current. However, the resistivity for graphene supported by a more rigid substrate is also smaller due to the shorter distance between the atoms in contact and their neighboring atoms. The combined effects of these factors result in the observed trends in current for the three substrate cases studied here.

4. Conclusion

The purpose of this study was to isolate the effect of the substrate on the contact conductivity of graphene as measured using AFM. Three systems were selected to capture the range of mechanical substrate support, from no substrate to elastic substrate to rigid substrate. In experiments, conductivity measurements were performed with the same AFM tip on free-standing graphene and graphene supported by PDMS and UNCD. Analysis of the results indicated that, at all normal forces except the smallest measured, current was the largest for the free-standing graphene and the smallest for the UNCD-supported graphene. These experiments were complemented by simulations of free-standing graphene, graphite and graphene supported by diamond. The simulations showed similar current vs. normal force trends, with the more rigid substrate having the smallest current. To understand these results, the simulations were used to calculate the change in atomic contact area as a function of normal force. As expected, contact area exhibited similar trends as the current. Therefore, the results were fit to a continuum contact mechanics theory, which enabled calculation of the effective elastic moduli for the three cases. This analysis suggested that the elasticity of the substrate has a significant effect on current because it determines the size of the contact. However, differences between the relative current and the relative contact area of the three cases indicated that factors other than elasticity may be contributing to observations of the current change. Fitting of the simulation data to classical conduction theories suggested that the resistivity of the interface might be smaller for the more rigid substrate. This was rationalized by the effect of strain on conduction, and the concept was supported by calculations of the atom-atom distance within the graphene and across the interface, which were smaller for the more rigid substrate.

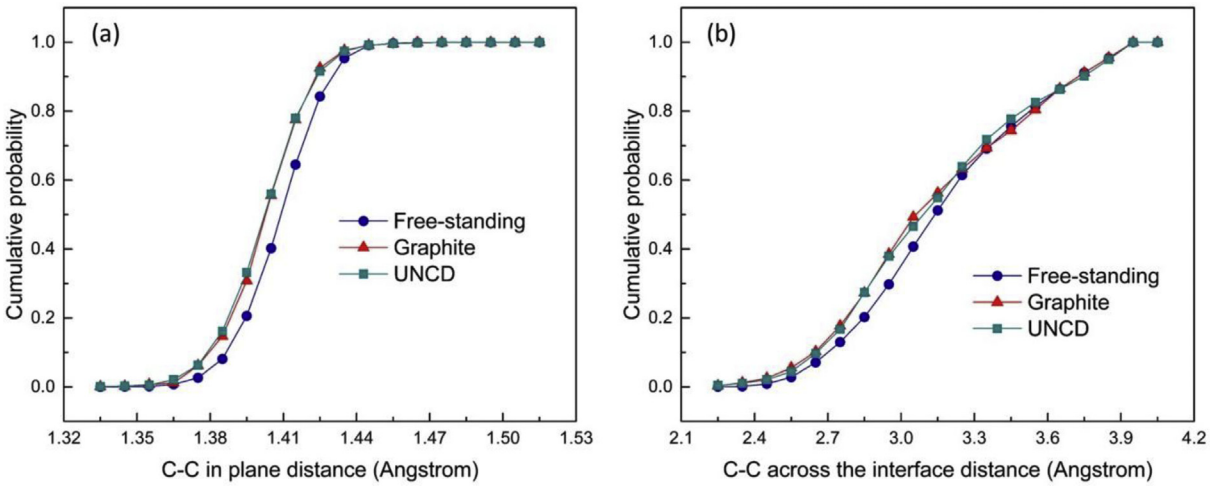

Fig. 8. Simulation results of cumulative distribution of (a) the in-plane distance between atoms within the graphene in the contact area and (b) the distance between graphene atoms in the contact and their closest neighbor in the tip. (A colour version of this figure can be viewed online.)

Therefore, the influence of a substrate on graphene conductivity is two-fold: the dominant factor is the effective elasticity of the contact, which determines contact size, and the secondary factor is the effect of the substrate on atom-atom distances in the contact, which determines resistivity. These findings have important implications for understanding conductive AFM measurements, as well as potentially for tuning the electrical contact conductance through variations in the mechanical properties of the substrate.

Acknowledgements

This research was supported by the Air Force Office of Scientific Research Award No. FA9550-15-1-0256.

This work was performed in part at the University of North Texas's Materials Research Facility. Support from Advanced Materials and Manufacturing Processes Institute at University of North Texas is appreciated.

References

[1] D. Berman, A. Erdemir, A.V. Sumant, Graphene: a new emerging lubricant, Mater. Today 17 (1) (2014) 31–42.
[2] D. Berman, S.A. Deshmukh, S.K.R.S. Sankaranarayanan, A. Erdemir, A.V. Sumant, Extraordinary macroscale wear resistance of one atom thick graphene layer, Adv. Funct. Mater. 24 (42) (2014) 6640–6646.
[3] S. Li, Q. Li, R.W. Carpick, P. Gumbsch, X.Z. Liu, X. Ding, J. Sun, J. Li, The evolving quality of frictional contact with graphene, Nature 539 (2016) 541–545.
[4] E.J. Sandoz-Rosado, O.A. Tertuliano, E.J. Terrell, An atomistic study of the abrasive wear and failure of graphene sheets when used as a solid lubricant and a comparison to diamond-like-carbon coatings, Carbon 50 (2012) 4078–4084.
[5] C.E.E. Rao, A.E. Sood, K.E. Subrahmanyam, A. Govindaraj, Graphene: the new two-dimensional nanomaterial, Angew. Chem. Int. Ed. 48 (2009) 7752–7777.
[6] M. Kalbacova, A. Broz, J. Kong, M. Kalbac, Graphene substrates promote adherence of human osteoblasts and mesenchymal stromal cells, Carbon 48 (2010) 4323–4329.
[7] F. Xia, T. Mueller, R. Golizadeh-Mojarad, M. Freitag, Y.M. Lin, J. Tsang, V. Perebeinos, P. Avouris, Photocurrent imaging and efficient photon detection in a graphene transistor, Nano Lett. 9 (2009) 1039–1044.
[8] J.S. Bunch, A.M.V.D. Zande, S.S. Verbridge, I.W. Frank, D.M. Tanenbaum, J.M. Parpia, H.G. Craighead, P.L. McEuen, Electromechanical resonators from graphene sheets, Science 315 (2007) 490–493.
[9] T. Ramanathan, A.A. Abdala, S. Stankovich, D.A. Dikin, M. Herrera-Alonso, R.D. Piner, D.H. Adamson, H.C. Schniepp, X. Chen, R.S. Ruoff, S.T. Nguyen, I.A. Aksay, R.K. Prud'Homme, L.C. Brinson, Functionalized graphene sheets for polymer nanocomposites, Nat. Nanotechnol. 3 (2008) 491–495.
[10] H. Chang, L. Tang, Y. Wang, J. Jiang, J. Li, Graphene fluorescence resonance energy transfer aptasensor for the thrombin detection, Anal. Chem. 82 (2010) 2341–2346.
[11] D. Berman, S.A. Deshmukh, B. Narayanan, S.K.R.S. Sankaranarayanan, Z. Yan, A.A. Balandin, A. Zinovev, D. Rosenmann, A.V. Sumant, Metal-induced rapid transformation of diamond into single and multilayer graphene on wafer scale, Nat. Commun. 12099 (2016).
[12] X. Du, I. Skachko, A. Barker, E.Y. Andrei, Approaching ballistic transport in suspended graphene, Nat. Nanotechnol. 3 (2008) 491–495.
[13] Q.H. Wang, Z. Jin, K.K. Kim, A.J. Hilmer, G.L. Paulus, C.J. Shih, M. Ham, J. Sanchez-Yamagishi, K. Watanabe, T. Taniguchi, J. Kong, P. Jarillo-Herrero, M. Strano, Understanding and controlling the substrate effect on graphene electron-transfer chemistry via reactivity imprint lithography, Nat. Chem. 4 (2012) 724–732.
[14] S. Son, C. Holroyd, J. Clough, A. Horn, S.P.K. Koehler, C. Casiraghi, Substrate dependence of graphene reactivity towards hydrogenation, Appl. Phys. Lett. 109 (2016) 243103.
[15] F. Varchon, R. Feng, J. Hass, X. Li, B.N. Nguyen, C. Naud, P. Mallet, J.-Y. Veuillen, C. Berger, E.H. Conrad, Electronic structure of epitaxial graphene layers on SiC: effect of the substrate, Phys. Rev. Lett. 99 (2007) 126805.
[16] Y.Y. Wang, Z.H. Ni, T. Yu, Z.X. Shen, H.M. Wang, Y.H. Wu, W. Chen, A.T.S. Wee, Raman studies of monolayer graphene: the substrate effect, J. Phys. Chem. C 112 (2008).
[17] G. Paolicelli, M. Tripathi, V. Corradini, A. Candini, S. Valeri, Nanoscale frictional behavior of graphene on SiO2 and Ni (111) substrates, Nanotechnology 26 (2015) 055703.
[18] J. Lee, X. Hu, A.A. Voevodin, A. Martini, D. Berman, Effect of substrate support on dynamic graphene/metal electrical contacts, Micromachines 9 (4) (2018) 169.
[19] T.D. Jacobs, A. Martini, Measuring and understanding contact area at the nanoscale: a review, Appl. Mech. Rev. 69 (2017), 060802.
[20] M. Enachescu, R.J.A.v.d. Oetelaar, R.W. Carpick, D.F. Ogletree, C.F.J. Flipse, M. Salmeron, Atomic force microscopy study of an ideally hard contact: the diamond(111)/tungsten carbide interface, Phys. Rev. Lett. 81 (1998) 1877–1880.
[21] P.E. Marszalek, W.J. Greenleaf, H. Li, A.F. Oberhauser, J.M. Fernandez, Atomic force microscopy captures quantized plastic deformation in gold nanowires, Proc. Natl. Acad. Sci. 97 (2000) 6282–6286.
[22] D.J. Oliver, J. Maassen, M.E. Ouali, W. Paul, T. Hagedorn, Y. Miyahara, Y. Qi, H. Guo, P. Grütter, Conductivity of an atomically defined metallic interface, Proc. Natl. Acad. Sci. 109 (2012) 19097–19102.
[23] P.N. Nirmalraj, T. Lutz, S. Kumar, G.S. Duesberg, J.J. Boland, Nanoscale mapping of electrical resistivity and connectivity in graphene strips and networks, Nano Lett. 11 (2010) 16–22.
[24] S.H. Ji, J.B. Hannon, R.M. Tromp, V. Perebeinos, J. Tersoff, Atomic-scale transport in epitaxial graphene, Nat. Mater. 11 (2012) 114–119.
[25] N. Onofrio, A. Strachan, Voltage equilibration for reactive atomistic simulations of electrochemical processes, J. Chem. Phys. 143 (2015) 054109.
[26] N. Onofrio, D. Guzman, A. Strachan, Atomic origin of ultrafast resistance switching in nanoscale electrometallization cells, Nat. Mater. 14 (2015) 440–446.
[27] W.B. Yang, X.F. Lu, Z.X. Cao, Growth of nanocrystalline diamond protective coatings on quartz glass, J. Appl. Phys. 91 (2002) 10068–10073.
[28] Y. Hu, J.D. Mackenzie, Structure-related mechanical properties of ormosils by SOL-GEL process, MRS Proceedings 271 (1992) 681–686.
[29] Y. Bao, W. Wang, Y. Zhou, Investigation of the relationship between elastic modulus and hardness based on depth-sensing indentation measurements, Acta Mater. 52 (18) (2004) 5397–5404.
[30] J. Musil, F. Kunc, H. Zeman, H. Polakova, Relationships between hardness, Young's modulus and elastic recovery in hard nanocomposite coatings, Surf.

Coating. Technol. 154 (2–3) (2002) 304–313.
[31] P. May, Y.A. Mankelevich, Experiment and modeling of the deposition of ultrananocrystalline diamond films using hot filament chemical vapor deposition and Ar/ CH 4/ H 2 gas mixtures: a generalized mechanism for ultrananocrystalline diamond growth, J. Appl. Phys. 100 (2) (2006) 024301.
[32] C. Lee, X. Wei, J.W. Kysar, J. Hone, Measurement of the elastic properties and intrinsic strength of monolayer graphene, Science 321 (5887) (2008) 385–388.
[33] G.-H. Lee, R.C. Cooper, S.J. An, S. Lee, A. van der Zande, N. Petrone, A.G. Hammerberg, C. Lee, B. Crawford, W. Oliver, J.W. Kysar, J. Hone, High-strength chemical-vapor–deposited graphene and grain boundaries, Science 340 (6136) (2013) 1073–1076.
[34] S.G. Srinivasan, A.C.v. Duin, P. Ganesh, Development of a ReaxFF potential for carbon condensed phases and its application to the thermal fragmentation of a large fullerene, J. Phys. Chem. A 119 (2015) 571–580.
[35] S. Plimpton, Fast parallel algorithms for short-range molecular dynamics, J. Comput. Phys. 117 (1995) 1–19.
[36] X. Hu, A. Martini, Atomistic simulations of contact area and conductance at nanoscale interfaces, Nanoscale 9 (2017) 16852–16857.
[37] N. Onofrio, D. Guzman, A. Strachan, Atomistic simulations of electrochemical metallization cells: mechanisms of ultra-fast resistance switching in nanoscale devices, Nanoscale 8 (2016) 14037–14047.
[38] K.L. Johnson, K. Kendall, A.D. Roberts, Surface energy and the contact of elastic solids, Proc. R. Soc. A 324 (1971) 301–313.
[39] Y. Gao, S. Kim, S. Zhou, H.C. Chiu, D. Nélias, C. Berger, W. Heer, L. Polloni, R. Sordan, A. Bongiorno, E. Riedo, Elastic coupling between layers in two-dimensional materials, Nat. Mater. 14 (2015) 714–720.
[40] O.L. Blakslee, D.G. Proctor, E.J. Seldin, G.B. Spence, T. Weng, Elastic constants of compression-annealed pyrolytic graphite, J. Appl. Phys. 41 (1970) 3373–3382.
[41] B. Hajgató, S. Güryel, Y. Dauphin, J.M. Blairon, H.E. Miltner, G.V. Lier, F.D. Proft, P. Geerlings, Out-of-plane shear and out-of plane Young's modulus of double-layer graphene, Chem. Phys. Lett. 564 (2013) 37–40.
[42] L. Banszerus, M. Schmitz, S. Engels, M. Goldsche, K. Watanabe, T. Taniguchi, B. Beschoten, C. Stampfer, Ballistic transport exceeding 28 μm in CVD grown graphene, Nano Lett. 16 (2016) 1387–1391.
[43] P.G. Slade, Electrical Contacts: Principles and Applications, CRC press, 2017.
[44] S.H. Bae, Y. Lee, B.K. Sharma, H.J. Lee, J.H. Kim, J.H. Ahn, Graphene-based transparent strain sensor, Carbon 51 (2013) 236–242.
[45] J. Zhao, C. He, R. Yang, Z. Shi, M. Cheng, W. Yang, G. Xie, D. Wang, D. Shi, G. Zhang, Ultra-sensitive strain sensors based on piezoresistive nanographene films, Appl. Phys. Lett. 101 (2012) 063112.
[46] H. Tian, Y. Shu, Y.L. Cui, W.T. Mi, Y. Yang, D. Xie, T.L. Ren, Scalable fabrication of high-performance and flexible graphene strain sensors, Nanoscale 6 (2014) 699–705.
[47] X.W. Fu, Z.M. Liao, J.X. Zhou, Y.B. Zhou, H.C. Wu, R. Zhang, G. Jing, J. Xu, X. Wu, W. Guo, D. Yu, Strain dependent resistance in chemical vapor deposition grown graphene, Appl. Phys. Lett. 99 (2011) 213107.
[48] M. Topsaka, V.M.K. Bagci, S. Ciraci, Current-voltage (I-V) characteristics of armchair graphene nanoribbons under uniaxial strain, Phys. Rev. B 81 (2010) 205437.
[49] J.G. Simmons, Generalized formula for the electric tunnel effect between similar electrodes separated by a thin insulating film, J. Appl. Phys. 34 (1963) 1793–1803.
[50] J.G. Simmons, Electric tunnel effect between dissimilar electrodes separated by a thin insulating film, J. Appl. Phys. 34 (1963) 2581–2590.